Jurnal Ilmu Fisika
Vol. 15, No. 2, September 2023, pp. 91-105
ISSN: 1979-4657 (Print); 2614-7386 (Online)
https://doi.org/10.25077/jif.15.2.91-105.2023

Jurnal Ilmu Fisika
Open Access

Synthesis of Fluorescent Carbon Dots (CDs) Using Laser Ablation Method for Bioimaging Application

Jumardin Jumardin[1], Akhiruddin Maddu[2], Kokoeh Santoso[3], Isnaeni Isnaeni [4]

[1] Department of Physics, Faculty of Sciences and Technology, Alauddin State Islamic University of Makassar Gowa, 92113, Indonesia
[2] Department of Physics, Faculty of Mathematics and Natural Sciences, IPB University, Bogor, 16680, Indonesia
[3] Department of Anatomy, Physiology and Pharmacology, School of Veterinary and Biomedical, IPB University Bogor, 16680, Indonesia
[4] Research Center for Photonics, National Research and Innovation Agency (Badan Riset dan Inovasi Nasional, BRIN) BJ Habibie Science and Technology Park, Banten 15314, Indonesia

Article Info

Article History:

Received January 17, 2023
Revised March 12, 2023
Accepted April 19, 2023
Published online May 06, 2023

Keywords:

Carbon dots
Laser ablation
Fluoresccent
Bioimaging

Corresponding Author:

Jumardin Jumardin
Email: jumardin.jumardin@uin-alauddin.ac.id

ABSTRACT

Carbon Dots (CDs) were synthesized using laser ablation by focusing the laser beam on carbon (Tea) material in colloid (CH_3) for 3 hours. UV-Vis spectroscopic and fluorometric characterization showed absorption of the wavelength peaks caused by the control treatment and after laser ablation and coating using Poly Ethylene Glycol (PEG_{400}). The excitation and emission energies are formulations of CDs absorbance wavelength and fluorescence intensity. The absorbance coefficient is obtained based on the absorbance value of the cuvette thickness. The transmittance value (T) is obtained based on the absorption coefficient multiplied by 100%. CD fluorescence wavelength based on control parameters was 489 nm. After laser ablation was 496 nm, and after coating was 511 nm. CDs morphology and size characteristics are 4 nm to 10 nm based on TEM measurements. Fluorescence analysis for bioimaging applications on the luminescence intensity value of internalized blue CDs in zebrafish eye organs. The average intensity of CDs in the eye organs, gill, intestinal, dorsal, and tail injection points was 88.15 %, 91.58 %, 92.76 %, and 0.00 %.

1. INTRODUCTION

Residing in the nanoscale realm, Carbon Dots (CDs) are celebrated for their robust photoluminescence, excellent biocompatibility, and minimal cellular toxicity, earmarking them as stellar candidates for bioimaging pursuits (Liang et al., 2020; Alkian et al., 2022; Dias et al., 2019; Emam et al., 2017; Li et al., 2020). These nanomaterials, typically under 10 nm in size, emit visible light upon absorbing radiant energy—a process ignited by electron excitation to higher energy states followed by photon emission as the electrons revert to their original state (Zhang et al., 2021; Wang et al., 2009).

The intrinsic fluorescence of CDs, capable of being fine-tuned for various biological contexts, provides a versatile toolkit for the enhanced specificity and sensitivity required in diagnostic imaging (Phukan et al., 2022). This luminescence is pivotal in life sciences, aiding in the precise localization and quantification of biomolecules under the microscope, facilitating cellular analysis via flow-cytometry,

and enabling the measurement of molecular interactions in microplate assays (Mizuno et al., 2021; Wilson & Baietto, 2009; Galbusera et al., 2020; Nozeret et al., 2019).

Confocal Laser Scanning Microscopy (CLSM) emerges as a pivotal instrument in bioimaging, assessing the fluorescence intensity of CDs across various wavelengths to unveil cellular uptake (He et al., 2018; Jiang et al., 2015). This sophisticated microscopy serves as a cornerstone for characterizing CDs' applications, propelling forward our comprehension of their interactions within biological systems (Kaczmarek et al., 2021). Notably, research by Kang and colleagues elucidated the distribution of CDs within zebrafish embryos, highlighting the versatility of these nanoparticles (Kang et al., 2015). In this nano realm, CDs, including Graphene Quantum Dots (GQDs) and Carbonized Polymer Dots (CPDs), boast distinct morphologies and structures, with diameters confined to the nanometer scale (Biswal & Bhatia, 2021; Kumar et al., 2020; Wu et al., 2021; R. Wang et al., 2021).

Our research focuses on the dispersion patterns of fluorescent CDs within zebrafish's ocular systems, exploring various injection sites to discern distribution dynamics. Leveraging the precision of laser ablation—a process devoid of excess chemicals—this method employs a laser to meticulously craft micro-features from a target material (Jiang et al., 2022). Utilizing a 1064 nm Nd:YAG laser, we pursue the synthesis of CDs, delving into their optical characteristics, morphology, and size (Kaczmarek et al., 2021; Reyes et al., 2016). We meticulously quantify the energy absorption of CDs pre and post laser ablation, and upon integration with PEG400, adopting ImageJ for fluorescence intensity analysis in zebrafish ocular regions (Aji et al., 2017; Putro et al., 2019; Gao et al., 2020). Employing the Corrected Total Cell Fluorescence (CTCF) technique, we assess the fluorescence density across multiple image slices acquired via CLSM (Jakic et al., 2017), thereby enhancing our understanding of CDs' potential in bioimaging.

2. METHOD

2.1 Materials and Methods of Synthesis

The initial step involves manufacturing carbon materials by inserting up to 250 g (Tea) into the carbonization tool via a thermal furnace. Carbon materials are produced at a starting temperature of 25 °C and a final temperature of 900 °C, with a heating rate of 600 °C/h achieved through temperature elevation over a 3-hour period (Vinsiah & Suharman, 2014). Carbon materials are produced at a starting temperature of 25 °C and a final temperature of 900 °C, with a heating rate of 600 °C/h achieved through temperature elevation over a 3-hour period (Vinsiah & Suharman, 2014). Later, the carbon is pulverized to a powder size using a mortar before the application of laser ablation treatment. The process of laser ablation utilized in the production of CDs employs a Q Switch Nd: YAG Q Smart 850 model that operates at a frequency of 10 Hz and a wavelength of 1064 nm (Kim et al., 2017). The pulse width measures ±6 ns, and the energy output is 60 mJ.

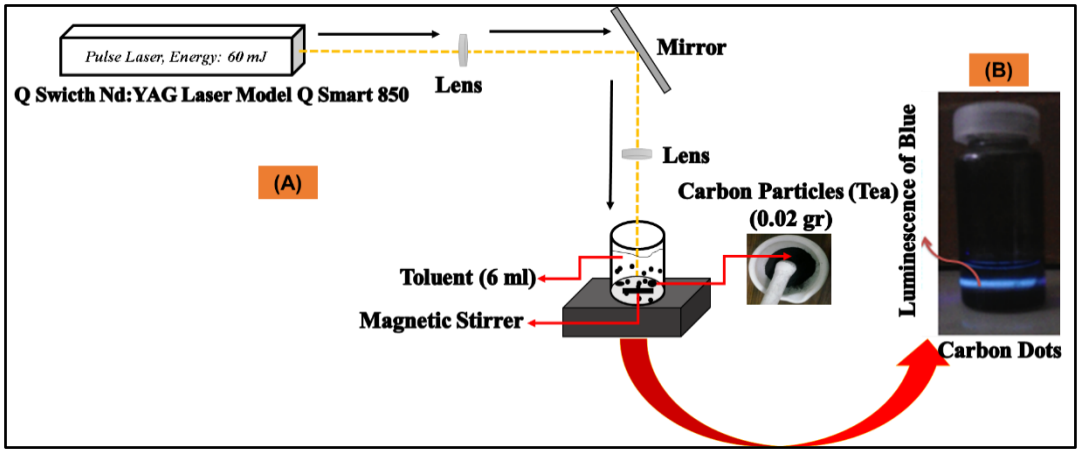

Figure 1 (a) CDs synthesis by laser ablation method and (b) Luminance of CDs.

The weight concentration of carbon is 0.02 g in 6 ml of toluene solvent (CH_3). Toluene is a transparent liquid that does not dissolve in water and evaporates in open air and water conditions. It has moderate, long-term toxicity to aquatic life (Khan et al., 2019). The synthesis process takes between 0 and 3 hours. The synthesis process involves using laser ablation for 3 hours, as depicted in Figure 1.

2.2 Characterization Method

In the second step, we utilize UV-Vis spectrophotometry to determine the absorbance intensity and wavelength absorbance of the optical properties. Next, we measure the fluorescence intensity of the wavelength peak of the CDs by means of spectrofluorometric, using a 405 nm laser. Furthermore, we measured the energy (E) of the CDs samples before and after laser ablation treatment using the following equation:

$$E = \frac{h.v}{\lambda} \quad . \tag{1}$$

We determined the energy (hv) based on the wavelengths (λ) of absorption (excitation) and fluorescence (emission) using Equation (1). The absorption coefficient (α) can be calculated in cm^{-1} units as follows:

$$\alpha = \frac{2{,}303.A}{d}, \tag{2}$$

where A represents the absorbance value (a.u) and d represents the cuvette diameter (cm). Based on α (Equation 2), we determined the value of the transmission spectrum (T):

$$T = 10^{-A}.100\% \ . \tag{3}$$

Thus, a comparative analysis between T and λ values can be conducted. The surface morphology of CDs was characterized using Transmission Electron Microscopy (TEM), and the CD sample (1 mg/ml) was placed into the TEM measurement vessel. Morphological imaging of CDs was conducted at 50 and 20 nm magnification.

The following step is the CD coating procedure utilizing polyethylene glycol (PEG_{400}). To dry the CD, 2 ml are evaporated and placed in a measuring beaker on a hotplate at 110.6°C. Then, add 1 mg/ml of Chloroform ($CHCl_3$) and 0.5 mg/ml of PEG_{400}. Dilute once again on the hotplate at 182°C and evaporate until the solution is dry on the measuring cup. Lastly, add 10 ml of Aquabides solvent, dilute, and leave for 20 minutes (Peng et al., 2020). Figure 2 displays the synthesis and coating steps.

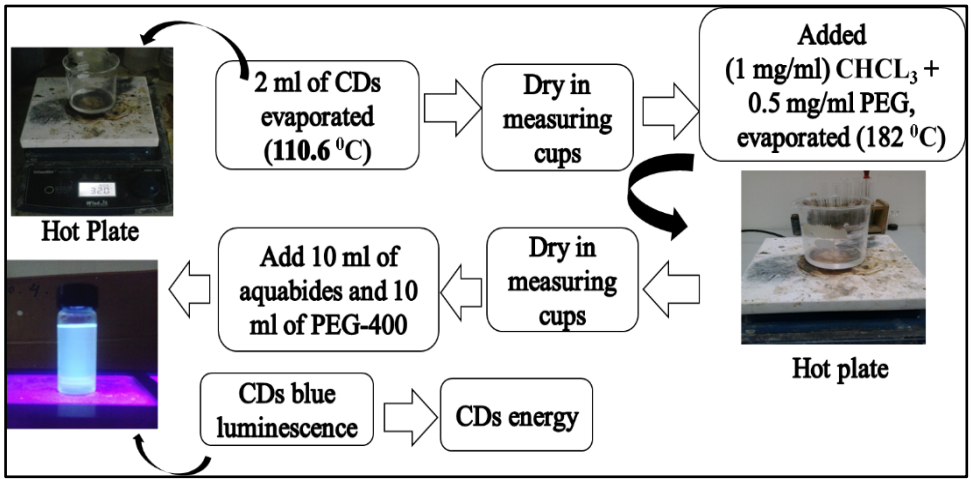

Figure 2 Methods for synthesis and coating of CDs with PEG_{400} and $CHCl_3$.

The final result was adding 10 ml of PEG_{400} as a solvent which can increase the spread and stability of CDs fluorescence in the blood circulation system of zebrafish animal models (Pal et al.,

2018). PEG_{400} is one type of carrier often used in a formulation to increase the solubility of materials that are difficult to dissolve. PEG_{400} liquid is clear, viscous, colorless, or practical, has a weak characteristic odor, is slightly hygroscopic, has a high degree of solubility in water, in ethanol (95%) in acetone, in other glycols, and aromatic hydrocarbons, practically insoluble in ether and aliphatic hydrocarbons. Characterization of optical properties (absorbance and fluorescence) was carried out again to determine the change in the peak wavelength of the emission after being coated with PEG_{400} and $CHCl_3$ and to calculate the change in transition energy in the shift of the peak wavelength of the CDs using Equation (1).

2.3 Injection Method in Animal Model (Zebrafish) with CDs

The fifth stage is injecting CDs into animal models (Zebrafish) and observing the fluorescence intensity of CDs using Confocal Laser Scanning Microscopy (DuMez et al., 2020). Injection method on Zebrafish (Gill, Intestinal, Dorsal, Tail) for four fish with the same dose (0.001 cc/ml). Observations using a confocal laser microscope to analyze the distribution of CDs fluorescence intensity of each Zebrafish in the eye organs. The anatomy of the injection point is shown in Figure 3.

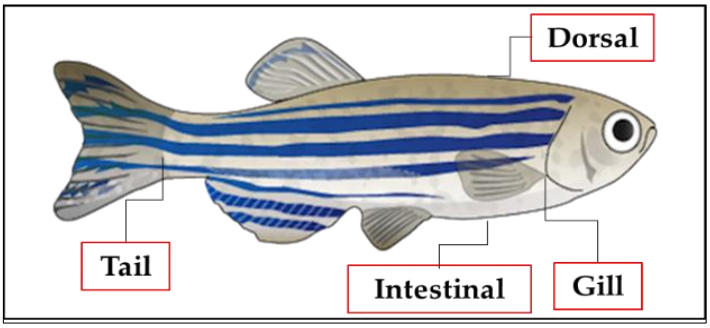

Figure 3 Zebrafish anatomy and CDs injection points (Hardianti et al., 2021).

Image slices or slice locations are recorded at 10x (100 µm) magnification for each focus of the observed eye object. The wavelength of the laser source used in CLSM microscopy (425-475) nm matches CDs emission wavelength (fluorescence). The critical process that needs to be performed is adjusting the emission laser source (405-600) nm of the CLSM tool to produce images with symmetrical magnification and focus on producing sharp fluorescence color resolution. The analytical pattern of the color distribution of each eye organ image was analyzed using the ImageJ software application (https:http://imagej.nih.gov/ij/). Figure 4(a) is the observation setup tool, and Figure 4(b) is the injection method.

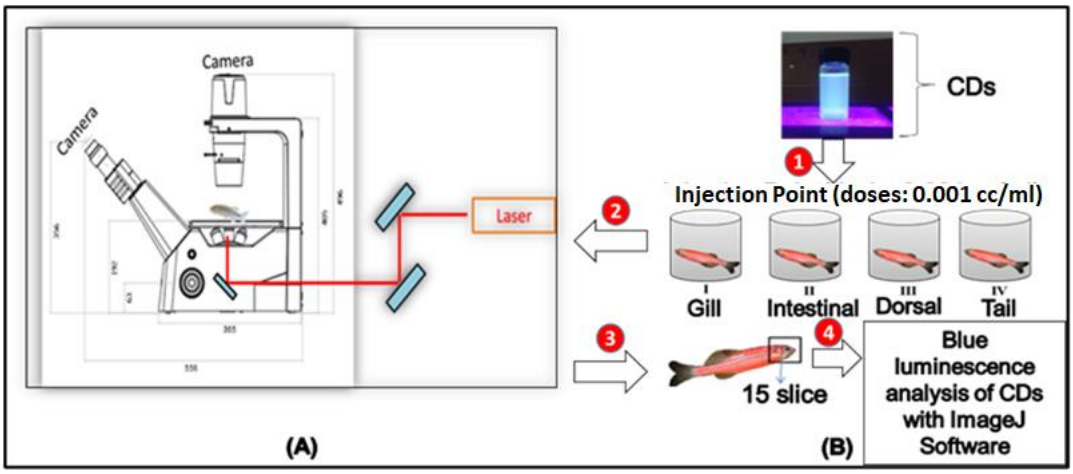

Figure 4 (a) Set up the CLSM tool and scan the CDs on Zebrafish eyes. (b) Injection method and luminescence analysis of CDs with ImageJ software.

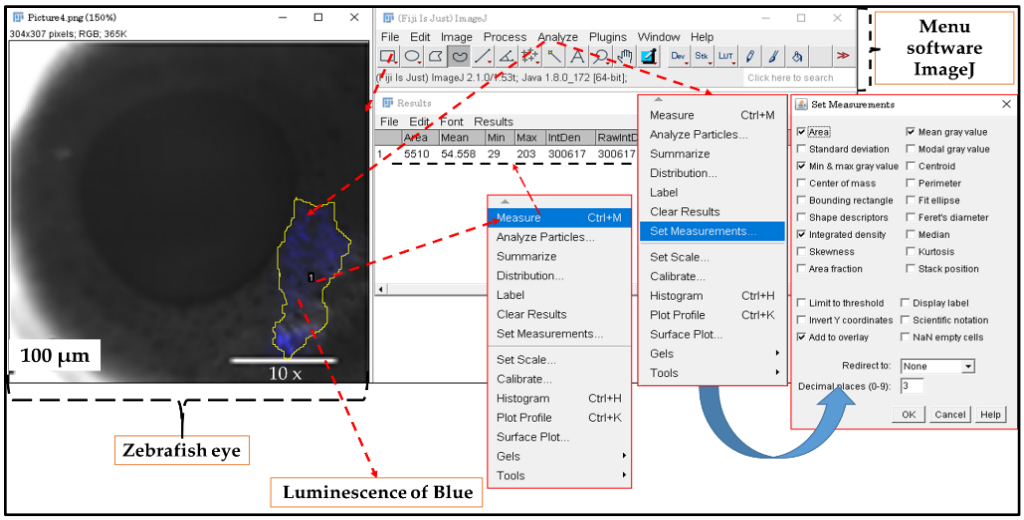

Figure 5 The method of measuring the area of the intensity of the blue colour CDs eye organs of Zebrafish with ImageJ software after going through CLSM observations.

To produce CDs that emit fluorescence in the fish's eye, open ImageJ software and choose the sequence of images obtained from the CLSM image (Figure 5). Slicing the sequence into a square shape from 1 to 15 is necessary. Go to the analysis menu to configure the measurement, integrated area intensity, and mean gray value. Select a region next to a cell with no blue fluorescent intensity, which serves as the background color. The corrected total cell fluorescence intensity calculation method (CTCF or Corrected Total Cell Fluorescence) uses the following equation:

$$CTCF = A - (BxD). \tag{4}$$

Component *A* represents the integrated density of blue pixels, *B* denotes the selected blue cell area, and *D* measures the mean fluorescence value of the background color in each image slice (Silic & Zhang, 2021).

3. RESULTS AND DISCUSSION

3.1 Optical Properties of CDs

Absorbance, fluorescence, and transmittance were measured before and after coating with PEG_{400} to determine changes in intensity and wavelength. The parameters of laser ablation and CDs coating were found to have no significant impact on the physical properties of the CDs. The spectrum color black represents the wavelength in the control treatment (CDs prior to undergoing Laser Ablation), while the color red indicates CDs treated with laser ablation and blue represents the spectrum of CDs coated using PEG_{400} via the evaporation method while heating. Laser ablation exposure of the CDs for 3 hours results in decreased transmittance, whereas PEG_{400} coating leads to increased transmittance.

Transmittance, fluorescence emission, and CD energy values were used as indicators for CLSM detection after treatment with PEG_{400}. CLSM is a tool that employs fluorescence and spatial filtration techniques to identify samples. This research employs CDs' fluorescent optical properties coated with PEG400 at emission wavelengths as a bio-imaging material. The filter automatically captures the emission wavelength based on the filter color (blue, green, yellow, and red). Then, the laser confocal microscope's emission wavelength selection is adjusted according to the CDs' emission wavelength.

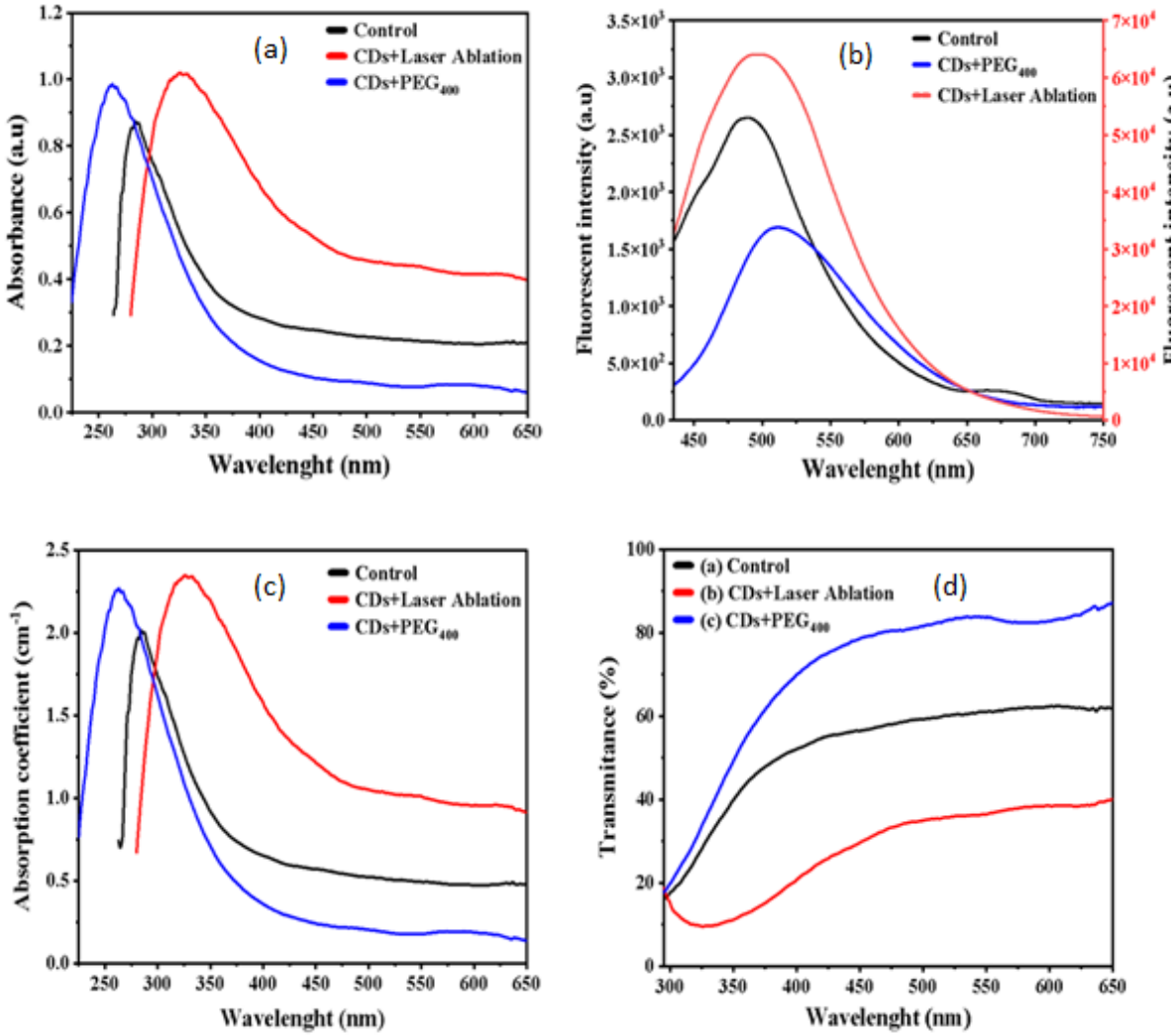

Figure 6 Wavelength spectrum (λ) to (a) absorbance value (a.u), (b) fluorescence intensity (a.u), (c) absorption coefficient and (d) CDs transmittance value before and after coating (coating) with PEG_{400}.

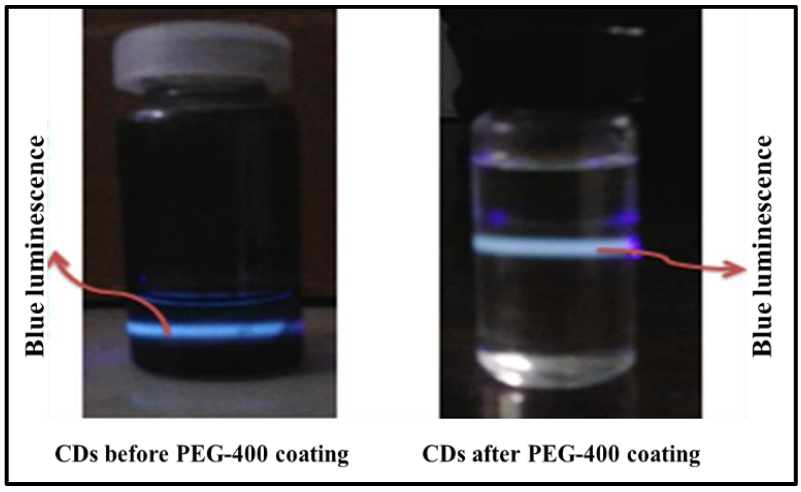

Figure 7 CDs of blue luminescence before and after coating with PEG_{400}.

Figure 6 (a) and 6 (b) display intensity and peak wavelength values of control, absorbance (excitation), and fluorescence (emission) of CDs before and after PEG_{400} coating. Figure 6 (c) and 6 (d) present the absorption and transmittance coefficients as well as the luminescence of the blue CDs (Figure 7). The peak wavelength change before and after PEG_{400} coating is represented in the absorbance results (Figure 7). The results suggest that the toluene (CH_3) CD molecules have stronger photon absorption intensity in the UV-Vis wavelength range before coating than the PEG_{400} molecules after coating. Changes in intensity values and shifts in wavelength can be observed for fluorescence, absorption coefficient, and transmittance. Table 1 displays data on absorbance, fluorescence intensity, absorption coefficient, transmittance, and associated values and energies.

Table 1 Intensity and wavelength of absorbance, fluorescence, transmittance, and energy of CDs.

Parameter	Absorbance		Fluorescence		Abs. Coef.	T	Energy Ex.	Energy Em.
	Int. (a.u)	Excitation λ, (nm)	Int. (a.u)	Emission λ, (nm)	cm^{-1}	(%)	(eV)	(eV)
(Control)	0.874	285	2645.94	489	2.01	13.36	4.35	2.54
(CDs+Laser Ablastion)	1.021	325	64001.7	496	2.35	9.52	3.81	2.50
(CDs+PEG_{400})	0.983	260	1689.27	511	2.26	10.39	4.76	2.43

Analyzing the transmission spectrum (T) at the given wavelength (λ) yields the absorption coefficient (α) as a wavelength function. Equations (2) and (3) establish the correlation curves between wavelength versus absorption coefficient (Figure 6(c)) and wavelength versus transmittance value (%) (Figure 6(d)). Emission (fluorescence) from CDs is optimized when photon absorption moves towards longer wavelengths or lower energies (Table 1). This phenomenon is a result of the discrepancy in electronic states of molecules upon photon irradiation. The discrepancy denotes the peak absorbance point due to photon absorption, resulting in a shift to shorter wavelengths or higher energies.

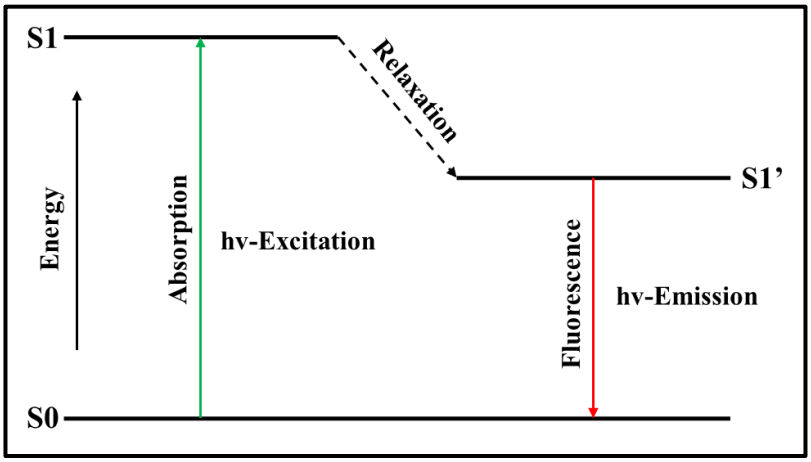

Figure 8 Mechanism of the CDs energy transition process.

CDs coated with PEG_{400} absorb photon energy, which leads to excitation to the LUMO (Lowest Unoccupied Molecular Orbital) level. The electrons then return to the ground state (S0) while emitting light to the HOMO (Highest Occupied Molecular Orbital) level. Prior to coating, the wavelength of CD emission was 496 nm, whereas it changed to 511 nm after coating as demonstrated in Table 1. The outcome suggests that PEG_{400} molecule has a greater absorption range of laser energy (405±10) nm as the light source in contrast with the primary solvent, Toluene (CH_3). When coated with PEG_{400}, the fluorescence intensity of CD was lower (1689.27 a.u) compared to the non-coated state (64001.7 a.u) (Figure 6 (b) and Table 1).

When the CDs return to their ground state (S0), as shown in Figure 8, they emit photons at energies of 4.35 eV, 3.81 eV, and 4.76 eV (*hv*-excitation). However, the emitted photons (*hv*-emission)

have lower energy levels at 2.54 eV, 2.50 eV, and 2.43 eV, as indicated in Table 1. Consequently, the CDs' molecules quickly become excited (relaxed) to the lowest vibrational energy level due to energy loss (dissipation) of the CDs. The structural differences between CDs in the ground state (S0) and the excited state (S1) result in the observed changes.

The wavelength's peak shift value suggests that laser confocal microscopy designed with electromagnetic wave optical instruments can induce photon absorption on CDs, thereby triggering their molecular compound activation for bioimaging purposes. According to Phan and Cho (2022), CD's luminescence energy for bioimaging applications of 0.5 eV corresponds with a CLSM microscope's emission wavelength. The laser ablation method utilized in the production of CDs generates energy with values of (2.4, 2.75, and 4.25) eV as reported by Isnaeni et al. (2019).

3.2 Morphology of CDs

TEM (Transmission Electron Microscopy) images of CDs at a scale of 50 nm (Figure 9(a)) exhibit no significant differences at a scale of 20 nm (as shown in Figure 9 (b)). Evaluation of the 20 nm scale indicates that the average size of CDs ranges from 4-10 nm in diameter, with a predominantly prevalent size distribution of 6 nm at the highest frequency percentage (%). A study utilizing laser ablation wavelengths produced consistent results, revealing a minute diameter of 0.22 nm using HR-TEM (Kaczmarek et al., 2021). The average diameter of CDs' size distribution is less than 50 nm, and its small spherical structure is visible only using the magnification scale on TEM, according to He et al. (2018). Based on image processing results using ImageJ software, CDs were examined using TEM to determine their nanoparticle morphology, structure, and size, as indicated by Rishi and Narinder (2015). Subsequently, ImageJ Software program was used to analyze the size of CDs nanoparticles based on the TEM image, as explained by Riyanto (2019).

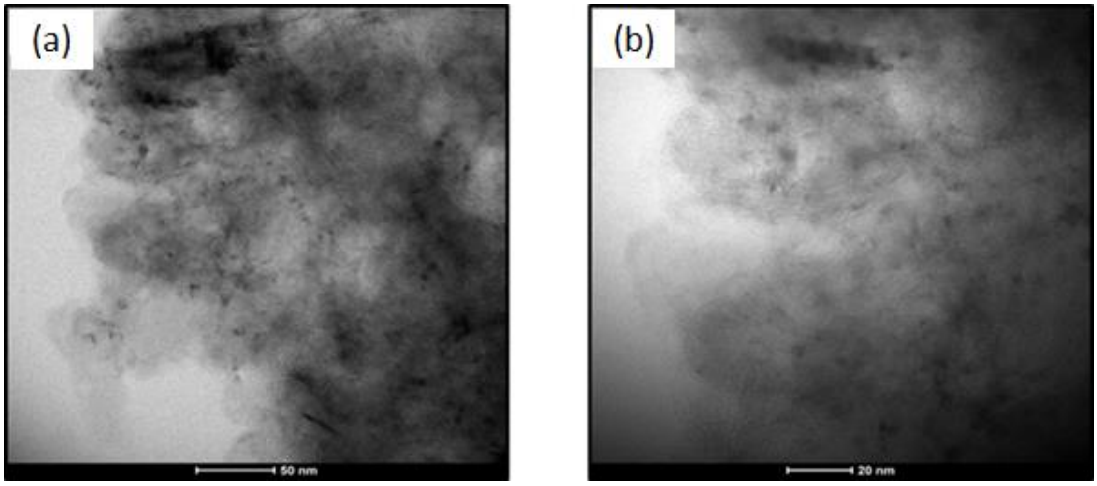

Figure 9 CDs morphology on the TEM measurement scale (a) 50 nm and (b) 20 nm.

3.3 CDs Luminescence in Zebrafish Eyes

Image of the Zebrafish eye organ captured in 15 slices with 10 times of magnification (100 μm scale), utilizing the CLSM microscope camera's spot at positions *x* (vertical) and *y* (horizontal). Figure 10, 11, 12, and 13 show the observations, and each slice represents a distinct injection point. The fifteen image slices are a product of CLSM's laser instrument penetration capacity through the Zebrafish eye organ. Identified the distribution of blue dots, which represent the fluorescence of compact discs on each horizontally and vertically recorded slice.

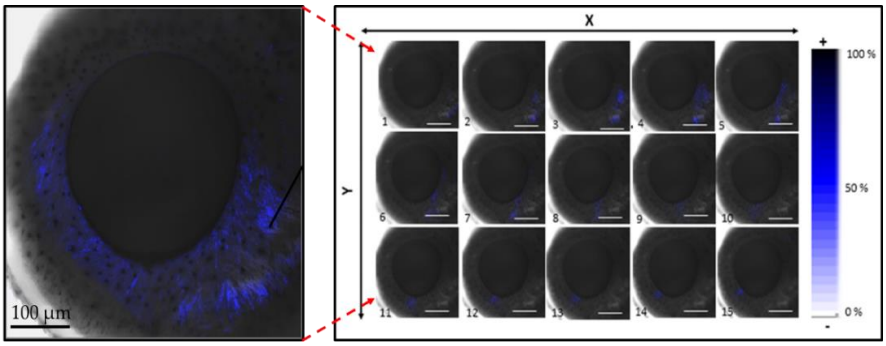

Figure 10 The blue luminescence image of the eye organ is based on 15 slices at the gill injection point of the eye Zebrafish organ.

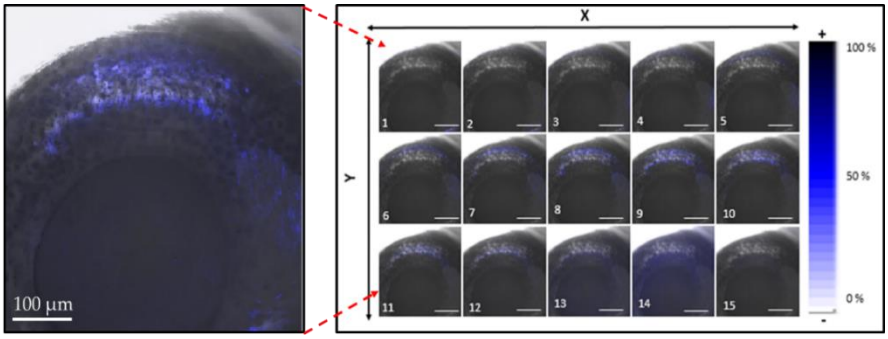

Figure 11 Same as Figure 10 but for the intestinal point of injection.

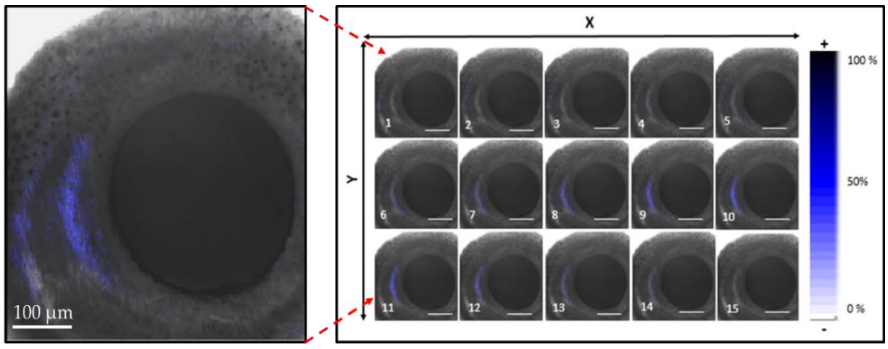

Figure 12 Same as Figure 10 but for the dorsal point injection.

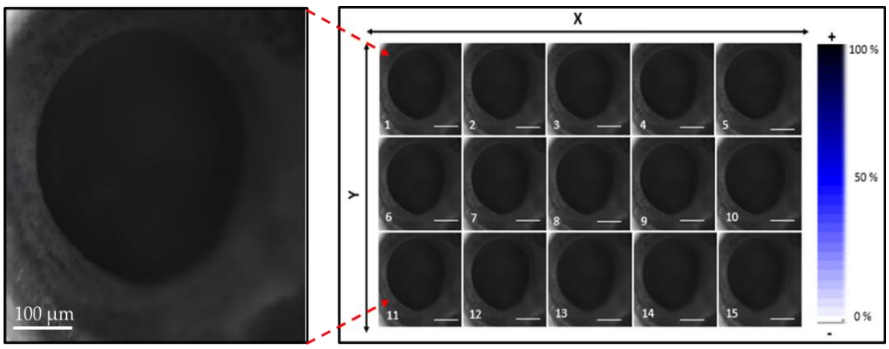

Figure 13 Same as Figure 10 but for the tail point injection.

The variation in injection points correlates with differences in CDs fluorescence intensity. This intensity is determined by the number of slice images captured by the confocal laser microscope on the Zebrafish eye, indicating variability in CDs molecules bound by the fish's blood circulation system. This intensity is determined by the number of slice images captured by the confocal laser microscope on the Zebrafish eye, indicating variability in CDs molecules bound by the fish's blood circulation system. Blue bleeding positions of the eye organ are presented in Figure 10, 11, 12, and 13 based on 15 slices obtained from various injection points. Figure 10 is an injection to the gill, Figure 11 is an injection to the intestine, Figure 12 is an injection to the dorsal, and Figure 13 is an injection to the tail.

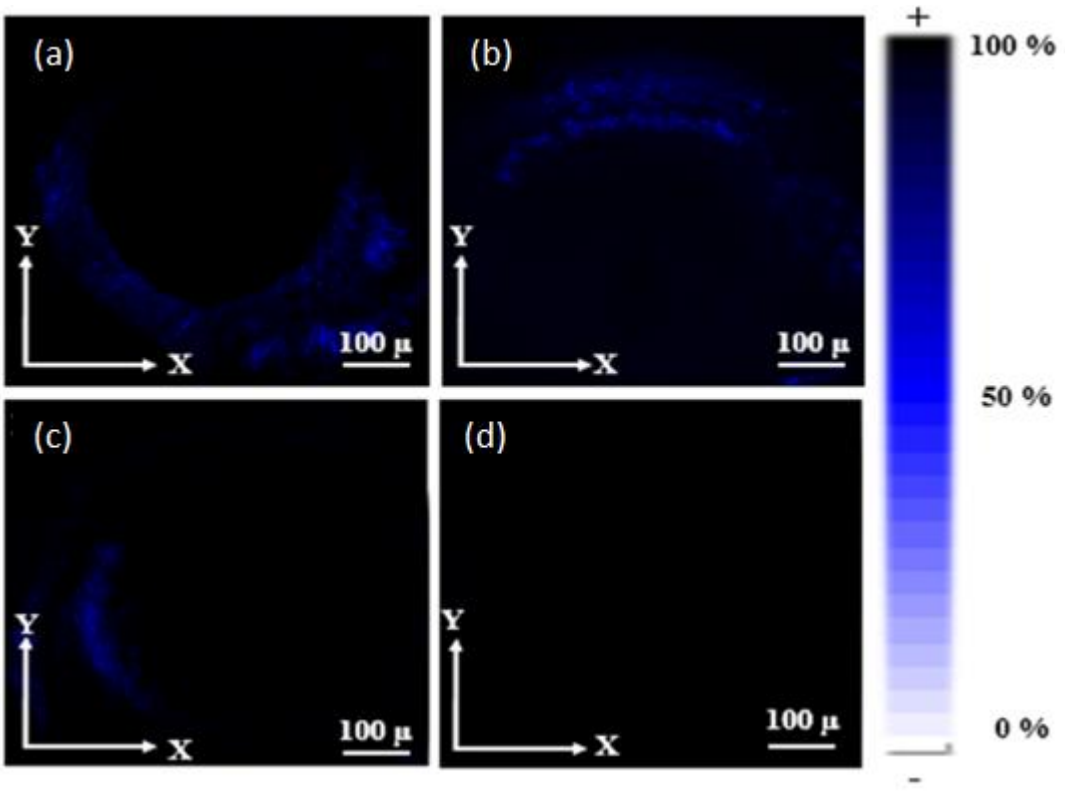

Figure 14 Distribution of CDs blue luminescence for combined 15 slices positions based on injection position in the eye (a: Gill injection, b: Intestinal injection, c: Dorsal, and d: Tail injection) in Zebrafish.

The CDs characteristics of each slice exhibited varying intensity levels of blue color (Figure 14). The luminescence of CDs detected in the Zebrafish eye organs expressed clear and strong intensity in comparison to each injection site as shown in Figure 14 (a), (b), (c), and (d). The quantitative evaluation of blue intensity of CDs in each of the 15 slices was measured using a pattern of black-pixel image and blue-pixel image. Figure 15(a) displays the luminescence intensity of the blue CDs in gill injection at 88.15%. The other images reveal the values accumulated sequentially from different injection points. Specifically, in Figure 14(b), the intestinal injection showed 91.58%, whereas dorsal injection in Figure 15(c) showed 92.76%. The Zebrafish tail injection exhibited a 0% value. This result occurred because, at 15 slices, the intensity of the blue fluorescence was not measured in the CLSM. The dye injected into the tail circulated through the old blood vessels and reached the eye's ring due to the heart located in the abdominal cavity of the Zebrafish. Figure 14 (d) shows that the scanning and laser firing method of confocal laser scanning microscopy (CLSM) did not indicate a blue glow for the tail injection.

Figure 15(a), (b), and (c) present a comparison of intensities based on the total fluorescence intensity in cells (CTCF) using Equation (4). Each image slice's characteristics reveal a difference in blue luminescence intensity of the CDs (refer to Figure 10, 11, 12, and 13). Table 2 outlines the method

of summing up the blue CDs luminescence intensity on 15 image slices of the Zebrafish eye organ. Each image slice is augmented by adding its CTCF intensity value and then averaged to determine a percentage value, based on the pixel density of each image (15 slices). Zebrafish possess a closed circulatory system. They have single blood circulation, since blood flows through the heart only once during one circulation. The zebrafish heart has an atrium and a chamber, forming two distinct chambers. Between the atrium and the ventricle lies a unidirectional valve responsible for blood drainage from the atrium to the ventricle (Dal et al., 2020).

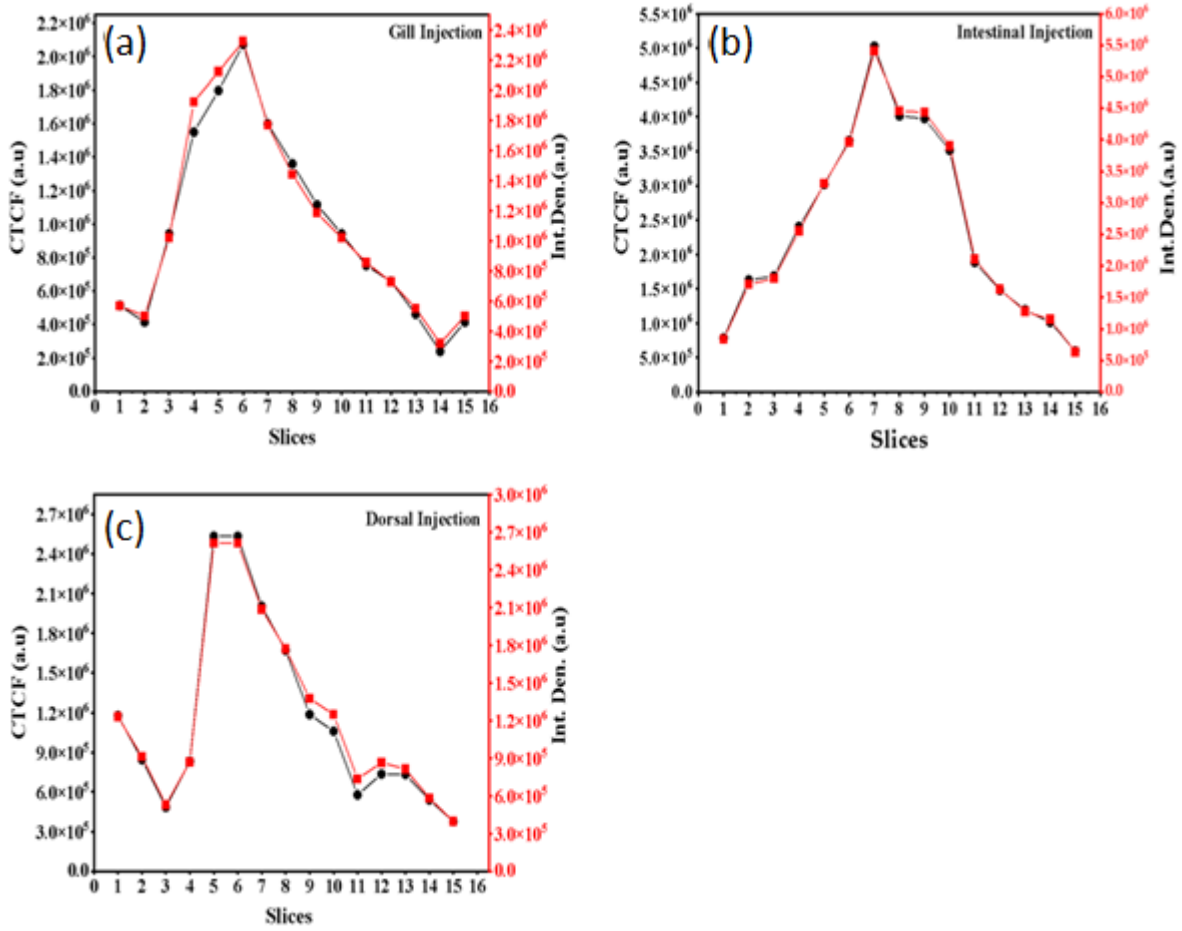

Figure 15 Graph of the relationship of 15 slices (image slices) to total fluorescent intensity (CTCF) and fluorescent density in zebrafish eye organ cells for gill (a), intestinal (b) and dorsal (b) injection.

Table 2 Accumulated CDs blue luminescence intensity at the injection point position.

Injection Point Position	Average intensity (a.u)		%
	Int.Density	CTCF	
Gill	1121410.27	988492.49	88.15
Intestinal	2612191.00	2392369.64	91.58
Dorsal	1208238.80	1120706.76	92.76
Tail	0.00	0.00	0.00

Table 2 illustrates the variations in the CDs molecules that bind to the Zebrafish circulatory system and highlights luminescence intensity at each injection point (CTCF). The Gill, Intestinal, Dorsal, and Tail regions, when subjected to injection, directly transfer the CDs molecules to the eye cavity. This occurrence is due to the heart's location in the abdominal cavity of the Zebrafish (Yuniarto

et al., 2017). The CDs-bound blood is pumped from the ventral aorta to the gills. At the location of the gill capillaries, the CDs molecules, which are bound by blood, flow towards the dorsal aorta in the eye and head regions, and subsequently to the capillaries dispersed throughout the caudal fin portions of the body. Finally, the CDs molecules return to the heart region. One notable characteristic of the Zebrafish is its transparent body, which can be imaged through bioimaging tomography and magnetic resonance imaging techniques (Gedda et al., 2021). Several previous studies have utilized Zebrafish as animal models for bio-imaging applications using various materials, including analyzing fluorescence imaging with labeling techniques on cancer cells injected into the bodies of Zebrafish (Ignatius & Langenau, 2009). Technical term abbreviations are explained when first used. Biased language is avoided, and formal register is maintained. Grammatical correctness is ensured at all times. In addition, Blackburn et al. (2011) observed the fluorescence intensity in adult zebrafish after injecting them with fluorescent material, resulting in the luminescence color being visible for each material. Consistent citation and footnote formatting are employed throughout the text.

The difference in value at the injection position shows a qualitative and quantitative comparison of CDs luminescence in the eye organs of Zebrafish. The difference occurs based on the nature of the CDs molecular compounds that are internalized into the Zebrafish organs after the CDs are coated with PEG_{400}. The fluorescence intensity of the CDs shows the difference in the CDs molecules bound by the Zebrafish blood circulation system. Moreover, the fluorescence intensity value of CDs determines the characteristics of CLSM. CDs are bioimaging materials with energy values and emission wavelengths that match the CLSM filter so that fluorescent luminescence in Zebrafish eye organs can be detected with different blue intensity values. Some similar studies that use CDs as bioimaging materials with zebrafish animal models are the distribution of CDs in Zebrafish embryos and larvae (Kang et al., 2015), observation of Zebrafish bones using CD fluorescence (Li et al., 2016) and fluorescence methods on CDs for biological labeling in bacteria, tumor cells, tissues, and organelles (Unnikrishnan et al., 2020).

4. CONCLUSION

The investigation of Carbon Dots (CDs) as luminescent materials, obtained from natural sources like tea, has shown potential for their use in bioimaging. Our study affirms that these CDs exhibit suitable energy values and emission wavelengths that align with Confocal Laser Scanning Microscopy (CLSM) filters. The study reveals that the blue luminescence of compact disks in the ocular tissue of zebrafish is detectable through varied levels of blue intensity seen across 15 image slices. Notably, the injection site's location was found to affect the intensity of blue luminescence, as reflected in the average Corrected Total Cell Fluorescence (CTCF) relative to the pixel density of the 15 slices within the zebrafish's eye. This characteristic highlights the practicality of naturally-derived CDs as a fluorescent dye for bioimaging applications. This marks a major advancement in non-toxic and biocompatible imaging methods.

REFERENCES

Aji, M. P., Susanto, Wiguna, P. A., & Sulhadi. (2017). Facile synthesis of luminescent carbon dots from mangosteen peel by pyrolysis method. *Journal of Theoretical and Applied Physics*, *11*(2), 119–126. https://doi.org/10.1007/s40094-017-0250-3

Alkian, I., Sutanto, H., & Hadiyanto. (2022). Quantum yield optimization of carbon dots using response surface methodology and its application as control of Fe 3+ ion levels in drinking water. *Materials Research Express*, *9*(1), 015702. https://doi.org/10.1088/2053-1591/ac3f60

Biswal, M. R., & Bhatia, S. (2021). Carbon Dot Nanoparticles: Exploring the Potential Use for Gene Delivery in Ophthalmic Diseases. *Nanomaterials*, *11*(4), 935. https://doi.org/10.3390/nano11040935

Blackburn, J. S., Liu, S., Raimondi, A. R., Ignatius, M. S., Salthouse, C. D., & Langenau, D. M. (2011). High-throughput imaging of adult fluorescent zebrafish with an LED fluorescence macroscope. *Nature Protocols*, *6*(2), 229–241. https://doi.org/10.1038/nprot.2010.170

Dal, N. K., Kocere, A., Wohlmann, J., Van Herck, S., Bauer, T. A., Resseguier, J., Bagherifam, S., Hyldmo, H., Barz, M., De Geest, B. G., & Fenaroli, F. (2020). Zebrafish Embryos Allow Prediction of Nanoparticle Circulation Times in Mice and Facilitate Quantification of Nanoparticle–Cell Interactions. *Small*, *16*(5), 1906719. https://doi.org/10.1002/smll.201906719

Dias, C., Vasimalai, N., P. Sárria, M., Pinheiro, I., Vilas-Boas, V., Peixoto, J., & Espiña, B. (2019). Biocompatibility and Bioimaging Potential of Fruit-Based Carbon Dots. *Nanomaterials*, *9*(2), 199. https://doi.org/10.3390/nano9020199

DuMez, R., Miyanji, E. H., Corado-Santiago, L., Barrameda, B., Zhou, Y., Hettiarachchi, S. D., Leblanc, R. M., & Skromne, I. (2020). Carbon dots deposition in adult bones reveal areas of growth, injury and regeneration. *Pharmacology and Toxicology*. https://doi.org/https://doi.org/10.1101/2020.10.13.338426

Emam, A. N., Loutfy, S. A., Mostafa, A. A., Awad, H., & Mohamed, M. B. (2017). Cyto-toxicity, biocompatibility and cellular response of carbon dots–plasmonic based nano-hybrids for bioimaging. *RSC Advances*, *7*(38), 23502–23514. https://doi.org/10.1039/C7RA01423F

Galbusera, L., Bellement-Theroue, G., Urchueguia, A., Julou, T., & van Nimwegen, E. (2020). Using fluorescence flow cytometry data for single-cell gene expression analysis in bacteria. *PLOS ONE*, *15*(10), e0240233. https://doi.org/10.1371/journal.pone.0240233

Gao, D., Barber, P. R., Chacko, J. V., Kader Sagar, M. A., Rueden, C. T., Grislis, A. R., Hiner, M. C., & Eliceiri, K. W. (2020). FLIMJ: An open-source ImageJ toolkit for fluorescence lifetime image data analysis. *PLOS ONE*, *15*(12), e0238327. https://doi.org/10.1371/journal.pone.0238327

Gedda, G., Bhupathi, A., & Balaji Gupta Tiruveedhi, V. L. N. (2021). Naturally Derived Carbon Dots as Bioimaging Agents. In *Biomechanics and Functional Tissue Engineering*. IntechOpen. https://doi.org/10.5772/intechopen.96912

Hardianti, M., Yuniarto, A., & Hasimun, P. (2021). Review: Zebrafish (Danio Rerio) Sebagai Model Obesitas dan Diabetes Melitus Tipe 2. *Jurnal Sains Farmasi & Klinis*, *8*(2), 69. https://doi.org/10.25077/jsfk.8.2.69-79.2021

He, H., Zheng, X., Liu, S., Zheng, M., Xie, Z., Wang, Y., Yu, M., & Shuai, X. (2018). Diketopyrrolopyrrole-based carbon dots for photodynamic therapy. *Nanoscale*, *10*(23), 10991–10998. https://doi.org/10.1039/C8NR02643B

He, M., Zhang, J., Wang, H., Kong, Y., Xiao, Y., & Xu, W. (2018). Material and Optical Properties of Fluorescent Carbon Quantum Dots Fabricated from Lemon Juice via Hydrothermal Reaction. *Nanoscale Research Letters*, *13*(1), 175. https://doi.org/10.1186/s11671-018-2581-7

Ignatius, M. S., & Langenau, D. M. (2009). Zebrafish as a Model for Cancer Self-Renewal. *Zebrafish*, *6*(4), 377–387. https://doi.org/10.1089/zeb.2009.0610

Isnaeni, Suliyanti, M. M., Shiddiq, M., & Sambudi, N. S. (2019). Optical Properties of Toluene-soluble Carbon Dots Prepared from Laser-ablated Coconut Fiber. *Makara Journal of Science*, *23*(4), 187–192. https://doi.org/10.7454/mss.v23i4.10639

Jakic, B., Buszko, M., Cappellano, G., & Wick, G. (2017). Elevated sodium leads to the increased expression of HSP60 and induces apoptosis in HUVECs. *PLOS ONE*, *12*(6), e0179383. https://doi.org/10.1371/journal.pone.0179383

Jiang, K., Sun, S., Zhang, L., Lu, Y., Wu, A., Cai, C., & Lin, H. (2015). Red, Green, and Blue Luminescence by Carbon Dots: Full-Color Emission Tuning and Multicolor Cellular Imaging. *Angewandte Chemie International Edition*, *54*(18), 5360–5363. https://doi.org/10.1002/anie.201501193

Jiang, Z., Li, L., Huang, H., He, W., & Ming, W. (2022). Progress in Laser Ablation and Biological Synthesis Processes: "Top-Down" and "Bottom-Up" Approaches for the Green Synthesis of Au/Ag Nanoparticles. *International Journal of Molecular Sciences*, *23*(23), 14658. https://doi.org/10.3390/ijms232314658

Kaczmarek, A., Hoffman, J., Morgiel, J., Mościcki, T., Stobiński, L., Szymański, Z., & Małolepszy, A. (2021). Luminescent Carbon Dots Synthesized by the Laser Ablation of Graphite in Polyethylenimine and Ethylenediamine. *Materials*, *14*(4), 729. https://doi.org/10.3390/ma14040729

Kang, Y.-F., Li, Y.-H., Fang, Y.-W., Xu, Y., Wei, X.-M., & Yin, X.-B. (2015). Carbon Quantum Dots for Zebrafish Fluorescence Imaging. *Scientific Reports*, *5*(1), 11835. https://doi.org/10.1038/srep11835

Khan, S., Newport, D., & Le Calvé, S. (2019). Development of a Toluene Detector Based on Deep UV Absorption Spectrophotometry Using Glass and Aluminum Capillary Tube Gas Cells with a LED Source. *Micromachines*, *10*(3), 193. https://doi.org/10.3390/mi10030193

Kim, M., Osone, S., Kim, T., Higashi, H., & Seto, T. (2017). Synthesis of Nanoparticles by Laser Ablation: A Review. *KONA Powder and Particle Journal*, *34*, 80–90. https://doi.org/10.14356/kona.2017009

Kumar, Y. R., Deshmukh, K., Sadasivuni, K. K., & Pasha, S. K. K. (2020). Graphene quantum dot based materials for sensing, bio-imaging and energy storage applications: a review. *RSC Advances*, *10*(40), 23861–23898. https://doi.org/10.1039/D0RA03938A

Li, H., Yan, X., Kong, D., Jin, R., Sun, C., Du, D., Lin, Y., & Lu, G. (2020). Recent advances in carbon dots for bioimaging applications. *Nanoscale Horizons*, *5*(2), 218–234. https://doi.org/10.1039/c9nh00476a

Li, S., Skromne, I., Peng, Z., Dallman, J., Al-Youbi, A. O., Bashammakh, A. S., El-Shahawi, M. S., & Leblanc, R. M. (2016). "Dark" carbon dots specifically "light-up" calcified zebrafish bones. *Journal of Materials Chemistry B*, *4*(46), 7398–7405. https://doi.org/10.1039/C6TB02241C

Liang, W., Bunker, C. E., & Sun, Y. P. (2020). Carbon Dots: Zero-Dimensional Carbon Allotrope with Unique Photoinduced Redox Characteristics. *ACS Omega*, *5*(2), 965–971. https://doi.org/10.1021/acsomega.9b03669

Mizuno, T., Hase, E., Minamikawa, T., Tokizane, Y., Oe, R., Koresawa, H., Yamamoto, H., & Yasui, T. (2021). Full-field fluorescence lifetime dual-comb microscopy using spectral mapping and frequency multiplexing of dual-comb optical beats. *Science Advances*, *7*(1). https://doi.org/10.1126/sciadv.abd2102

Nozeret, K., Boucharlat, A., Agou, F., & Buddelmeijer, N. (2019). A sensitive fluorescence-based assay to monitor enzymatic activity of the essential integral membrane protein Apolipoprotein N-acyltransferase (Lnt). *Scientific Reports*, *9*(1), 15978. https://doi.org/10.1038/s41598-019-52106-8

Pal, T., Mohiyuddin, S., & Packirisamy, G. (2018). Facile and Green Synthesis of Multicolor Fluorescence Carbon Dots from Curcumin: In Vitro and in Vivo Bioimaging and Other Applications. *ACS Omega*, *3*(1), 831–843. https://doi.org/10.1021/acsomega.7b01323

Peng, Z., Ji, C., Zhou, Y., Zhao, T., & Leblanc, R. M. (2020). Polyethylene glycol (PEG) derived carbon dots: Preparation and applications. *Applied Materials Today*, *20*, 100677. https://doi.org/10.1016/j.apmt.2020.100677

Phan, L. M. T., & Cho, S. (2022). Fluorescent Carbon Dot-Supported Imaging-Based Biomedicine: A Comprehensive Review. *Bioinorganic Chemistry and Applications*, *2022*, 1–32. https://doi.org/10.1155/2022/9303703

Phukan, K., Sarma, R. R., Dash, S., Devi, R., & Chowdhury, D. (2022). Carbon dot based nucleus targeted fluorescence imaging and detection of nuclear hydrogen peroxide in living cells. *Nanoscale Advances*, *4*(1), 138–149. https://doi.org/10.1039/D1NA00617G

Putro, P. A., Roza, L., & Isnaeni, I. (2019). THE EFFECT OF POLY (ETHYLENE GLYCOL) ON THE PHOTOLUMINESCENCE PROPERTIES OF CARBON DOTS FROM CASSAVA PEELS SYNTHESIZED BY HYDROTHERMAL METHODS. *Spektra: Jurnal Fisika Dan Aplikasinya*, *4*(1), 11–20. https://doi.org/10.21009/SPEKTRA.041.02

Reyes, D., Camacho, M., Camacho, M., Mayorga, M., Weathers, D., Salamo, G., Wang, Z., & Neogi, A. (2016). Laser Ablated Carbon Nanodots for Light Emission. *Nanoscale Research Letters*, *11*(1), 424. https://doi.org/10.1186/s11671-016-1638-8

Rishi, K., & Narinder, R. (2015). Particle Size and Shape Analysis using Imagej with Customized Tools for Segmentation of Particles. *International Journal of Engineering Research And*, *V4*(11). https://doi.org/10.17577/IJERTV4IS110211

Riyanto, A. (2019). Preparasi dan Karakteristik Fisis Nanopartikel Magnetit (Fe3O4). *Jurnal Fisika Flux: Jurnal Ilmiah Fisika FMIPA Universitas Lambung Mangkurat*, *16*(1), 35. https://doi.org/10.20527/flux.v16i1.5524

Silic, M. R., & Zhang, G. (2021). Tissue-specific modification of cellular bioelectrical activities using the chemogenetic tool, DREADD, in zebrafish. *Developmental Biology*. https://doi.org/10.1101/2021.06.22.449481

Unnikrishnan, B., Wu, R.-S., Wei, S.-C., Huang, C.-C., & Chang, H.-T. (2020). Fluorescent Carbon Dots for Selective Labeling of Subcellular Organelles. *ACS Omega*, *5*(20), 11248–11261. https://doi.org/10.1021/acsomega.9b04301

Vinsiah, R., & Suharman, A. (2014). Pembuatan Karbon Aktif dari Cangkang Kulit Buah Karet (Hevea brasilliensis). *Pendidikan Kimia Universitas Sriwijaya*, 189–199.

Wang, R., Gu, W., Liu, Z., Liu, Y., Ma, G., & Wei, J. (2021). Simple and Green Synthesis of Carbonized Polymer dots from Nylon 66 Waste Fibers and its Potential Application. *ACS Omega*, *6*(48), 32888–32895. https://doi.org/10.1021/acsomega.1c04808

Wang, X., Cao, L., Lu, F., Meziani, M. J., Li, H., Qi, G., Zhou, B., Harruff, B. A., Kermarrec, F., & Sun, Y.-P. (2009). Photoinduced electron transfers with carbon dots. *Chemical Communications*, *25*, 3774. https://doi.org/10.1039/b906252a

Wilson, A., & Baietto, M. (2009). Applications and Advances in Electronic-Nose Technologies. *Sensors*, *9*(7), 5099–5148. https://doi.org/10.3390/s90705099

Wu, Y., Li, C., van der Mei, H. C., Busscher, H. J., & Ren, Y. (2021). Carbon Quantum Dots Derived from Different Carbon Sources for Antibacterial Applications. *Antibiotics*, *10*(6), 623. https://doi.org/10.3390/antibiotics10060623

Yuniarto, A., Sukandar, E. Y., Fidrianny, I., & Adnyana, I. K. (2017). Aplikasi Zebrafish (Danio rerio) pada Beberapa Model Penyakit Eksperimental. *MPI (Media Pharmaceutica Indonesiana)*, *1*(3), 116–126. https://doi.org/10.24123/mpi.v1i3.215

Zhang, Q., Wang, R., Feng, B., Zhong, X., & Ostrikov, K. (2021). Photoluminescence mechanism of carbon dots: triggering high-color-purity red fluorescence emission through edge amino protonation. *Nature Communications*, *12*(1), 6856. https://doi.org/10.1038/s41467-021-27071-4